A novel system to explore the properties of graph model investigate the relationship between structural connectome and functional connectome

1. Introduction

Mapping neural connections holds promise for developing a better understanding of human's brain functions and neural computation (Deligianni et al, 2014). Connectome is a complete description of neural connections in humans' brain or nervous system. The connections can be divided to two types: the first type is known as structural connection, where it refers to the characterization of the axon fibre bundles structurally connect neural regions together; the second type, functional connection, is referred as the cross-region coordinated activity between two communicating regions (Clayden, 2013). The non-invasive nature and the superior resolution of soft tissues, makes magnetic resonance imaging(MRI), the most suitable and versatile modality in acquisition of information of connectivity based on either structural or functional connectomes (Shi et al, 2017).

Diffusion weighted MRI (dw-MRI) and resting-state functional MRI (rs-fMRI), allows researchers to acquire signals of structural and functional connectivity in which complementary information on brain structure and function is offered (Deligianni et al, 2013). Structural connectivity (SC) is indexed by measurements of the brain's white matter (WM) tracts microstructural properties via dw-MRI. The directional dependence of diffusion of water within the axon fibres, e.g. anisotropy, acts as the predominant property in reconstructing the WM tract's pathway between two coherent cortical regions (known as tractography). The produced "Streamline", is the connection of the reconstructed pathway in regions of interest(ROIs) using fibre tractography. The number of streamlines combined with fractional anisotropy (FA) that is used to measure fibre integrity, can be used to elaborate the representation of the human brain structural network (Contreras et al, 2015 ; Fjell et al, 2016). By contrast, functional connectivity (FC) refers to measurement of a degree of correlation between time series of neural activity in spatially distinct regions of grey matter. Rs-fMRI is the primary imaging technique in obtaining information of brain activity, and its signal intensity is dependent on the blood oxygen level in the active neuronal tissue (Contreras et al, 2015). In Biswal and his colleagues' landmarks experiments, they concluded that correlation of low frequency coherent spontaneous fluctuations of the signal intensity, manifests the FC of the fluctuation occurs at rest-state of the brain activity (Biswal et al, 1995). The differential FC between the rest state and the state in context of different stimuli or tasks, allows us to understand the dynamic changes of activity level in brain function along with the corresponding physiological conditions (Contreras et al, 2015).

Graph theoretical approach is considered as one of the most powerful analysis method in quantifying the brain's structural and functional network (Bullmore et al, 2009). This approach allows us to model the brain as a whole network, and also to infer effects of structural changes on the dynamic changes in brain function (Contreras et al, 2015). In the connectivity information based graph model, network is composed of a set of nodes denoting parcellated brain regions that are connected by edges representing connection like streamline (Bullmore et al, 2009). Since dw-MRI and rs-fMRI signals do not contain information about the direction, the connection in the graph model is undirected. Therefore, a symmetric matrix is used to represent the graph model, where the connection strength of the nodes is indicated by a series of weights (Clayden, 2013).

Previous studies have shown the significant correlations between rest state SC and FC, as corrections of the previously mentioned fluctuations among distinct cortical regions are coupled with the underlying SC. However, due to the respective technique limitations of the dw-MRI and the rs-MRI, and neither of them provides direct inference of connectivity, the relationship between SC and FC remains quite unclear and complex: a functional connection tend to be found in the structurally bonded regions, whereas structurally separate regions also show a functional connection (Chen et al, 2018; Clayden, 2013; Deco et al 2013). Various modelling and evaluation methods have been created so far, to predict FC weights from the associated SC weights, and finally utilize the results to explore the relationship between the SC and the FC between the two modalities within two ROIs (Chen et al, 2018; Deco et al 2013; Honey, 2009). A common problem with these studies, is that they only investigate certain properties of the graph model and explore specific form of the relationship. Therefore, a systematic study and comprehensive comparisons between the graph properties and the different forms of structure–function relationships are needed.

In this study, we aim to investigate how the graph properties of the connectomes are affected by selecting a certain parameter while

generating the connectomes, also use weights from graph models to find how structural connectome relates to functional connectome. This can be achieved by initially loading the datasets from TractorR software package (Clayden et al, 2011), defining the network nodes and calculate the metrics like edge density, shortest path length, efficiency and clustering coefficient; followed by estimating a continuous measure of association between nodes; then, collecting pairwise nodes associations to produce a association matrix and thresholding the individual matrix elements to generate an undirected graph; subsequently, calculating the parameters of interest in a particular graph model and comparing them with equivalent parameters of a subject in other models and the chosen ground truth; finally, evaluating and validating the fitting of the parameter of interest among all models (Bullmore et al, 2009).

2. Materials and Methods

2.1 Data source and pre-processing

Data for this study were divided into two parts according to their purposes of use. The first part of data is a multi-model imaging test dataset of a single healthy adult volunteer from TractorR Package, where structural connectomes derived from different anisotropy thresholds are also included. In addition, information of reconstructing the tractography is also contained in the tractor subdirectory of the first part data, their descriptions and the relevant use will be discussed further. The other part of data records 19 patients' weighted structural and functional connectomes. Its structural connectome was obtained by, weighting the average FA values in each voxel that is connected by streamline between pairwise cortical regions, with the number of streamlines connected to the voxel. By contrast, its functional connectome was derived from the normalization of the inverse covariance matrix. Images generated by a MRI scanner are generally stored as DICOM files and are subsequently converted to NIfTI-1 format (outputted with suffix ".nii") by the built-in Tractor R packages, so that these images can be read by associate Matlab Toolbox (Clayden et al, 2011; Rubinov et al, 2010).

2.2 Toolbox

Three Matlab toolboxes include Jimmy Shen's NIfTI toolbox, Brain Connectivity Toolbox(BCT) and Kevin Murphy's Matlab port of the corpcor R package, were used to perform the following tasks in order: loading of NIfTI-format images, calculation of graph metrics and estimation of correlation using a shrinkage approach (Rubinov & Sporns, 2010; Schäfer & Strimmer 2005; Shen et al, 2014).

2.3 Explore graph properties

2.3.1 FA map thresholding

Thresholding FA maps allow us to observe changes in spatial distribution of FA voxels. In the TractorR package, FA maps were determined by the diffusion tensor obtained from the estimation of the diffusion tensor model, which was based on raw diffusion-weighted data performed by ordinary or weighted least-squares regression (Basser et al. 1994; Clayden et al, 2011; Sinke et al, 2018). We initially loaded the preprocessed FA maps from the tractor directory in the TractorR package. Then, all the NaN (not a number) values and subthreshold values were set to 0 when the set of threshold value varied from 0.1 to 0.8 in a step size of 0.1. Finally, all the processed FA maps were stacked into 8 image stacks in gif format and were categorized based on the corresponding threshold value.

2.3.2 Graph matrices calculation

FA initially varied between 0.1 to 0.8 and in step size of 0.1, and the structural connectomes derived from the corresponding FA value from TractorR package were loaded. Then, the first 3 rows and columns of the structural connectome data matrix for each FA were discarded, and the remain matrix was used as the input to the built-in function from BCT, to calculate the graph matrices of interest for that connectome matrix. In the undirected connection density function created by Olaf Sporns, density_und, connection density (edge density) was found by finding ratio of actual edges in the graph to total number of possible edges. Mean shortest path is the mean number of edges have to be crossed on the shortest path from one node to another node. Distance matrix (distance_bin) created by Rubinov, was used to obtain distance matrix containing lengths of shortest paths between all pairs of nodes for each connectome. Then, for each connectome, the disconnected vertices (infinite) were not considered for computation. All the non-infinite (connected) distance matrix elements were summed up and divided by the number of connected elements, to obtain the mean shortest path. Efficiency_bin was the function used to compute efficiency for each connectome. Efficiency was computed by averaging the inverse of the shortest path length. Mean clustering coefficient was calculated by finding the mean fraction of the number of nearest neighbour connections exist around a

node over the maximum possible connections. This was achieved by using clustering_coef_bu function for each input structural connectome matrix derived from the corresponding FA (Bullmore et al, 2009; Fagiolo, 2007; Latora et al, 2001; Rubinov & Sporns, 2010; Watts and Strogatz, 1998).

2.3.3 Weighted functional connectome calculation

We initially loaded the cortical parcellation data transformed into the functional space, where there was a corresponding number labelling the coherent cortical region in each voxel. The rs-fMRI dataset pre-processed using FSL-FEAT was also loaded (Woolrich et al, 2001). Time courses varied between 1 to 15 in step size of 1, and the corresponding slice for each time step was stored. This slice was then averaged to create mean parcellation intensity at the corresponding parcellation value and time course. All the NaN values that indicates the disconnected vertices in the mean parcellation intensity matrix were removed and reshaped. Finally, this modified matrix was used as an input to covshrinkKPM function to get the covariance matrix, along with applying settings of varying lambda, adding binary threshold and not to shrinking the diagonal variance term on the covariance matrix, so that functional connectomes were obtained. The lambda varied from 0.1 to 0.8 in a step size of 0.1 in this case, hence a corresponding range of functional connectomes was produced for the use of getting the functional graph data.

2.4 Modelling relationships between connectomes

The relationship between structural and functional connectome was explored by predicting weights of functional connectivity between two brain regions I and j, f_{ij}, from weights of the associated structural connectivity, s_{ij} (Clayden, 2013).

2.4.1 Calculation of indirect structural connectivity

Initially, functional and structural connectome data were loaded by the built-in function, csvread. Then, we computed the indirect structural connectivity for each subject at voxel position (i,j), t_{ij}, using equation (1), where voxel indexes i and j varied from 1 to 68 on a step size of 1, and the subject index k varied from 1 to 19. This allowed us to obtain the maxima of the minimum weights.

$$t_{ij} = \max_k \{ \min \{ s_{ik}, s_{kj} \} \} \text{ s.t. } s_{ik}, s_{kj} \neq 0. \quad \text{Eqn(1)}$$

2.4.2 Model fitting and criteria evaluation

Five linear regression models, as shown in the Figure 1, and two devised models in Figure 2 were used to perform data fitting across all the 19 healthy subjects. Note that a_{ij}, β_{ij}, Y_{ij}, δ_{ij} and ϵ_{ij} are the coefficients for each edge if there is data, whereas δ_{ij} was computed by eqn(2) and ϵ_{ij} is the sum of all other 3 coefficients except δ_{ij}. The corresponding parameter of model fitting, x, for each coefficient from the left to the right are in increasing order starting from 0 until the highest order, e.g. x_0, x_1 and etc. To perform model fitting, we initially varied voxel indexes i and j from 1 to 68 on a step size of 1, obtained the indirect structural connectivity, three hob connectivity, structural and functional connectivity weights data, t_{ij}, s_{ij} and f_{ij}, and used them as inputs to models in Figure 1 and 2. We then found the best parameters by finding the minimum of unconstrained multivariable function with input of the function of the model and the model's starting points, where the starting points were obtained when we fit a single set of parameters for all edges. The outputs of the function minimization returned us each model's solution and objective function value at the solution. The solutions were then used as the coefficients of the parameters to estimate the fitting result of the model and the objective function values (f_eval) were divided by the product of the connectome's X and Y dimension (X*Y = 68*68 =4624), to find the average error. For 7 models with model index m from 1 to 7, the average error for each model were summed to find the corresponding residual sum of squares (RSS_m), and the RSS_m along with number of parameters(k_m) and number of subjects(n), were then utilized to compute that models' Akaike and Bayesian information criteria (AIC_m and BIC_m) as shown in equation(2) and (3).

$$\delta_{ij} = a_{ij} + \beta_{ij} \quad \text{Eqn(2)}$$

$$AIC_m = 2k_m + n \ln(RSS_m/n) \quad \text{Eqn(3)}$$

$$BIC_m = n \ln(RSS_m/n) + k_m \ln(n) \quad \text{Eqn(4)}$$

1. $f_{ij} = a + \beta\ s_{ij}$
2. $f_{ij} = a + \beta\ s_{ij} + \gamma\ s_{ij}^2$
3. $f_{ij} = a + \beta\ t_{ij}$
4. $f_{ij} = a + \beta\ t_{ij} + \gamma\ t_{ij}^2$
5. $f_{ij} = a + \beta\ s_{ij} + \gamma\ t_{ij}$

Figure 1. the linear regression model for data fitting

Combined:

6. $f_{ij} = \alpha_{ij} + \beta_{ij} * s_{ij} + \gamma * s_{ij}^2 + \delta * t_{ij} + \epsilon * t_{ij}^2$

Figure 2. the further model for investigating the connectome relationship

2.4.3 leave-one-out cross-validation

To compute leave-one-out cross validation error (LOO_XVE) for each edge, we initially obtained the connectivity weights like the previous sub session, but excluded the kth subject sets for each kind of connectivity weights. Then, the previous procedure of finding the best parameter and the average error was repeated, with the differences of: the output solution from the function minimisation using the non-excluded connectivity weights, was used as the parameters to the corresponding model; the previously excluded kth subject connectivity weights were used as the connectivity weights for model computation shown in Figure 1 and 2; both were combined to find the coefficients of error at kth subject (c_error_k) for each model. Finally, the LOO_XVE was calculated by $LOO\_XVE_{ij} = c\_error_k /k + LOO\_XVE_{ij\ at\ k\text{-}1}$ for varying subject index k from 1 to 19.

2.4.4 Model fitting for all edges

The previous fitting and evaluation procedures were repeated for all edges using a single set of coefficients, but for each model and for each subject independently. For subject index dependent fitting, the difference compared to the connection edge position dependent fitting, is that the kth subject's connectivity data were used for choosing the best parameters during varying the subject index k from 1 to 19, and average was found by f_eval/(X*Y*k) instead. By contrast, neither subject index nor edge position x and y index were varied in the model index dependent fitting, the difference to the edge model was produced by the computation in average error which equals to f_eval / X * Y * total number of subjects.

2.4.5 Correlation between connectivity

We initially estimated the connectivity density by summing the rows across each structural connectivity matrix, each functional connectivity matrix and each indirect structural connectivity matrix; followed by reshaping these matrices to matrices with dimensions of [total vertex length, total subject number] = [68,19]. Subsequently, we extracted the vth rows data each time during varying the vertex index (v) from 1 to 68. These extracted data were then used as input connectivity for model fitting and optimization, where the difference comes from the average error here was found by f_val / (v * total number of subjects). Finally, the solution produced by this modified fitting was used as the coefficients of the parameters. These coefficients were combined with the above input direct and indirect structural connectivity, using the models in Figure 1 and 2, to produce the estimated functional connectivity density. This density and the previously obtained functional connectivity density, were inputted to the Matlab corr2 function to find the correlation between them.

2.4.6 Relate structural and functional connections

The LASSO based multivariate linear model introduced by Deligianni and his colleagues, was used to relate each functional connection with a subset of structural connections (Deligianni et al., 2013). We used the lasso function implemented in the Matlab built-in package, to link the functional connection with the structural connection. Also, 10 fold cross validation (9 fold training sets and 1 fold validation set) were also performed on this model by adjusting settings in the lasso function, to examine the model's performance.

3. Results

3.1 Graph properties

3.1.1 Spatial distribution of voxels above threshold

The FA slice with the most significant spatial distribution variation above threshold across threshold values from 0.1 to 0.8, is present in Figure 3(a). Figure 3(b) indicates the mean ratio of number of voxels exceeds its threshold value to the total number of voxels across all FA data. Figure 3a shares the same characteristics as all other FA slices, which are: the higher the threshold value applied to the slice (the higher effective diffusivity), the fewer the FA voxels above threshold are remained (shown in Figure3(b)).

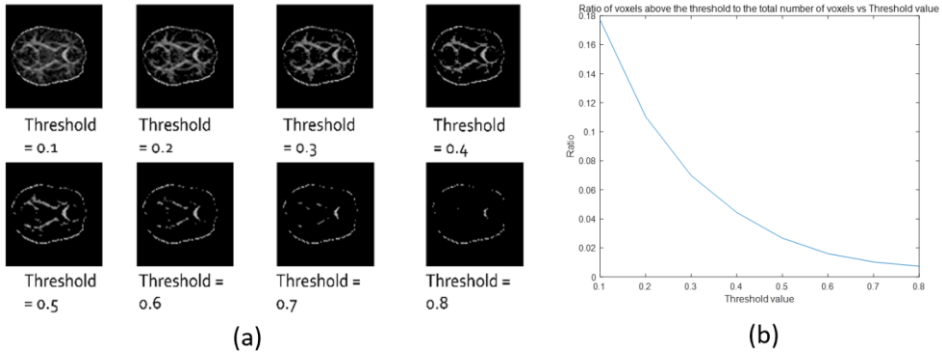

Figure 3. (a) Spatial distribution of FA voxels above threshold across the threshold values between 0.1 and 0.8 (b) Plot of ratio of number of voxels above the threshold to the total voxels number value against the corresponding threshold value

3.1.2 Network measurements

Both metrics for structural connectome and weighted functional connectome are calculated by combining the methods in 2.3.2-2.3.3. Density measures the ratio of actual edges to the possible edges, the density for structural and functional connectomes is shown in Figure 4 (a) and (e) respectively. Density variation with increasing threshold value in both graphs, have shown the general shape close to exponential decay, except for the discontinuous change for structural connection density observed at threshold value of 0.3 and 0.5. Same discontinuous change was also observed at the same threshold value in the mean shortest path, efficiency and mean clustering coefficients for structural connectome (Figure 4b,c and d), where mean shortest path measures the mean number of edges to be traversed from one node to another across all nodes, efficiency is inversely proportional to the shortest path and mean clustering coefficients measures the mean of the probability of a vertex's nearest neighbor vertices are connected. These observed discontinuous changes, reflect the network was fragmented into disconnected components. Similar to density graph in figure 4(e), other graph metrics for functional connectome also have an exponential variation, with a significant change at threshold value of 0.8 and graduate changes and more stable phases tend to appear at threshold value <=0.7. Hence, the appropriate threshold that reflects the structure correctly is given by the regions in 0.1-0.7 for functional connectome and 0.1-0.2 for structural connectome. In these stable regions, the network assemble the small world network characteristics of relatively small shortest path and larger mean clustering coefficients. Meanwhile, the overall trend of the metrics from Figure 4 (a) – (h) is decreasing, except the exponential increase in mean shortest path in Figure 4(f).

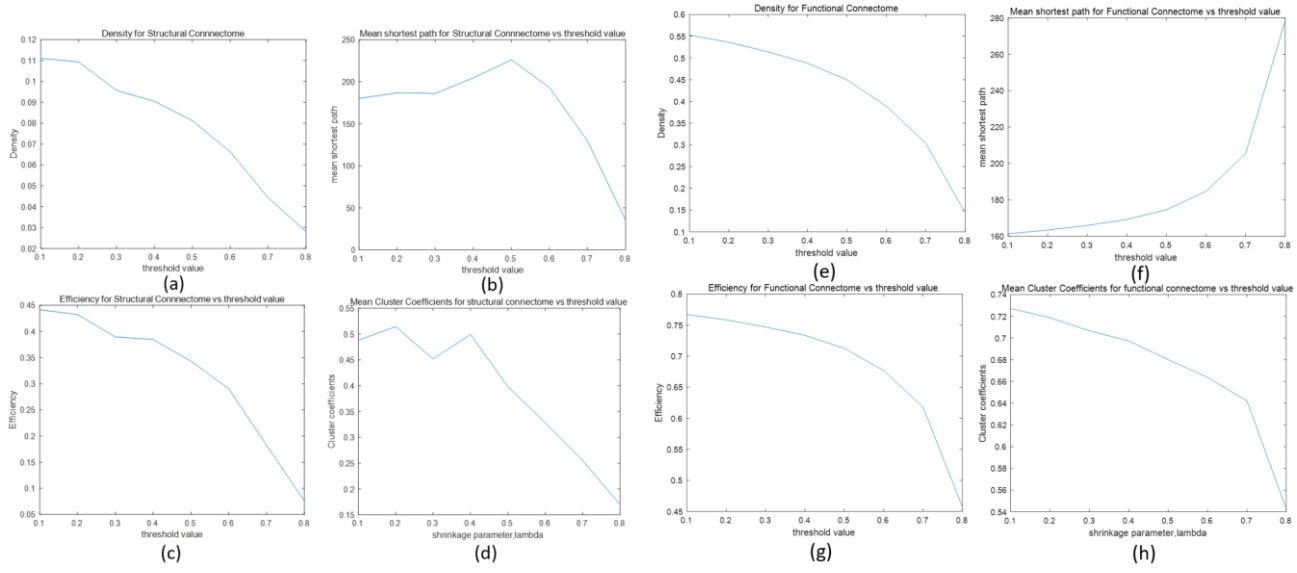

Figure 4 Network measurements, where (a)-(d) are the measurements for structural connectomes and (e)-(h) are the measurements for weighted functional connectomes.

3.2 Relationship between connectomes

3.2.1 Best-fitting model based on criteria evaluation across edges

Criteria evaluation including AIC,BIC and LOO_XVE provides comprehensive estimation of the quality of data fitting models, where such estimation balance the potential effect between model's parameter number(k_m) and residual errors. AIC estimates the relative distance between the data's unknown true likelihood function and the model's fitted likelihood function, and BIC provides the estimation of the Bayesian-based model's posterior probability of being true. Hence, a lower AIC value, represents the closer distance of a model to the truth; a lower BIC, represents the higher probability for a model to be the true model. Similarly, LOO_XVE is a type of cross validation estimating the generalisation error of the model trained on n-1 folds of data, where n is the total number of folds that the data is being divided. The generalization error related to how accurate the model will be when applied to other points, hence a smaller LOO_XVE value represents a more accurate model when applied to new points (Fabozzi et al, 2014).

Maps describing the distribution of the best-fitting model across each node, were created for each evaluation method (see Figure 5 AIC, BIC and LOO_XVE). The best-fitting model for the located connection depends on the minimum value obtained from its corresponding evaluation criteria, and is described by colours of red, green, blue, yellow or light blue to represent model of 1-5 respectively. From Figure 5, we can observe that model 1 and 3 occupy the most space in AIC and BIC map, whereas the best-fitting model in most nodes in LOO_XVE is model 2. The individual plot of each criteria across different edges for each model is shown in Figure 6, where each plots' title includes the model number and the corresponding criteria sum value across all the nodes. Through Figure 6, we observed that model 1 and 3 give the same and minimum values for AIC,BIC and LOO_XVE. This implies that model 1 and 3 are the 2 best-fitting models in terms of the space coverage and the overall performance across nodes. By contrast, model 2 is powerful for the covered regions in the best fitting map for LOO_XVE, but its performance in its non-covering regions of the map is poorer than others.

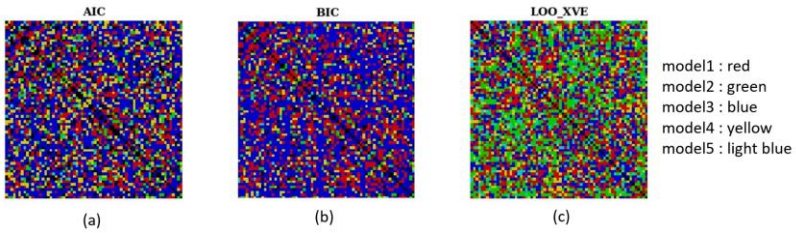

Figure 5. The maps to describe the best fitting model across each node by evaluation quantity of : (a)AIC, (b) BIC and (c) Leave one out cross validation error

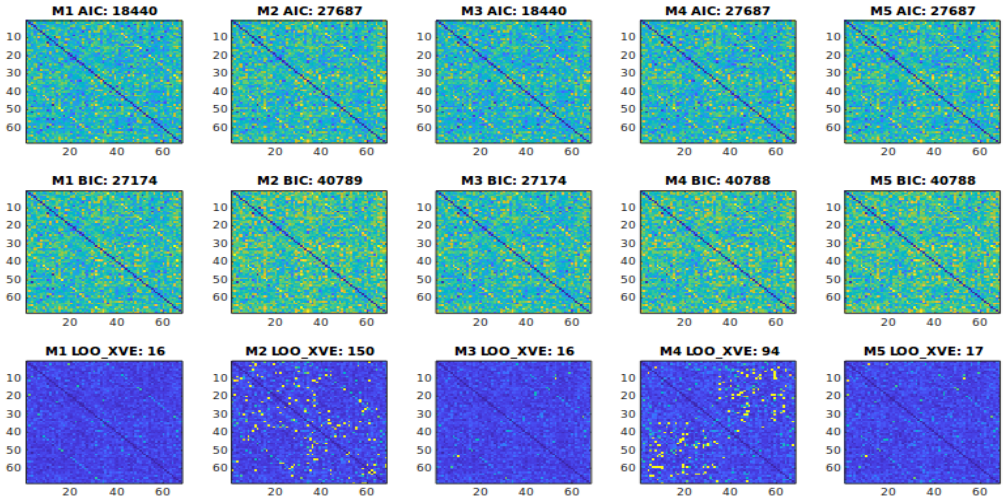

Figure 6. Individual plots of the evaluation criteria values across all nodes for 5 basic models, where these criteria are AIC,BIC and LOO_XVE

3.2.2 Best fitting model based on RSS evaluation

If the balance between the parameter number and the resultant error is not considered, then the evaluation based on RSS or sum of squared errors can be used to identify the model with the highest accuracy without considering the effect from the parameter number. Figure 7 (a) shows the RSS of each model, and model 4 gives the minimum RSS. Therefore, model 4 is inferred to be the most accurate model among 5 basics models, as a smaller RSS corresponds to a higher accuracy. Then, finding the voxel positions with small and large error in the average error matrix of model 4, the resultant fitting of 19 subjects for two connection that holds particularly strongly (at [22,20]) and weakly (at [50,16]), and the corresponding RSS, is presented in Figure 7 (b) and (c) respectively. This validates that the fitting accuracy is directly proportional to the RSS.

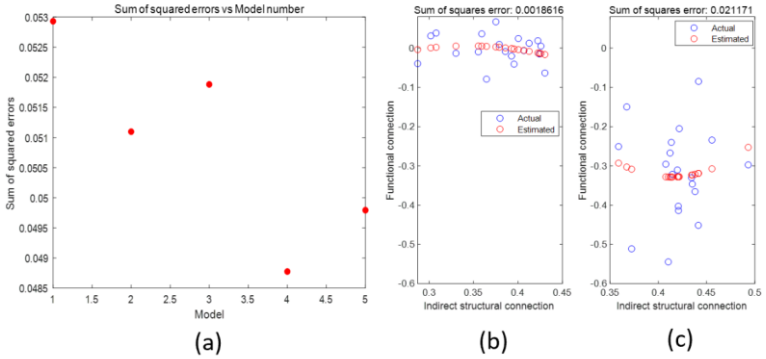

Figure 7. the plots evaluate the data fitting quality based on sum of squared errors (or RSS), where (a) shows the RSS across 5 basic models, (b) and (c) shows the fitting for T and F that holds strongly and weakly

3.2.3 Total fitting with single coefficients over all edges

The previous evaluation methods were repeated with fitting a single set of coefficients over all edges, for each model and for each subject respectively. Table 1 summarises the evaluation criteria values produced by fitting the single set of coefficients over all edges for each model, the corresponding criteria rank and overall rank of all the six models. In agreement with the AIC and BIC results in Figure 6, model 1 and model 3 in Table 1 are the top 2 models giving the smallest AIC and BIC values. However, in contradiction with the fitting results of LOO_XVE for each edge, model 6 and 5 are the best two single coefficients fitting models for all edges in terms of LOO_XVE as shown in Table 1. The sum of RSS across all edges (total RSS) for each model equals to LOO_XVE of that model, hence model 6 and 5 are the two most accurate models for fitting for all edges, as a smaller total RSS represents there are more overlap points between the empirical connectivity data and the simulated ones. This finding is supported by the observation of the fitting plot in Figure 8 (a). Likewise, similar evaluation methods were also applied to each independent subject. Figure 8(b) shows the variation of the mean criteria quantities with increasing subject index. In this figure, we observed that, the mean LOO_XVE that is equivalent to the mean of total RSS, stays stable across all subject index, this indicates that the LOO_XVE and the RSS is independent of the subject index. Also, the mean AIC and the BIC were observed to gradually decrease with the increasing subject index. This indicates that AIC and BIC are inversely proportional to the subject index.

model	AIC		BIC		LOO_XVE		Sum	Rank
1	-70.75	1	-68.86	1	90.43	4	-49.18	1
2	-69.00	4	-66.17	4	89.248	3	-45.93	4
3	-70.40	2	-68.51	2	92.124	6	-46.79	2
4	-68.492	5	-65.658	5	91.696	5	-42.45	5
5	-69.017	3	-66.184	3	89.189	2	-46.01	3
6	-65.458	6	-60.736	6	87.170	1	-39.02	6

Table 1. The evaluation criteria and the corresponding rank for basic and additional devised models

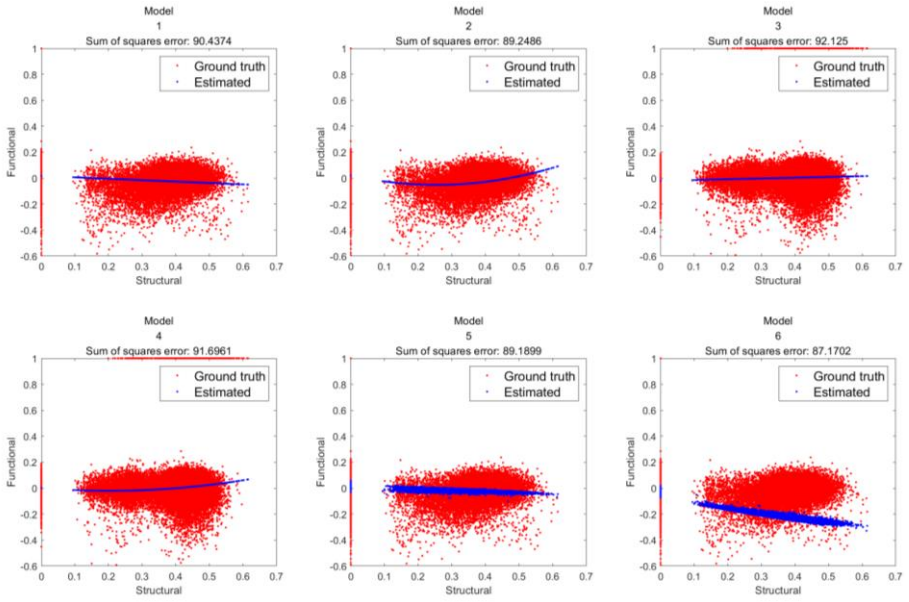

(a)

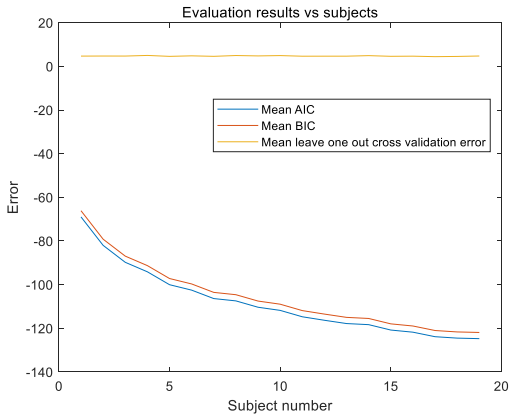

(b)

Figure 8 (a). Total fitting with single coefficients for all edges, for model 1-6. (b) The means of evaluation criteria quantities for fitting with single coefficients for all edges across subjects

3.2.4 Connectivity vertex density association

Figure 9 shows the model-wised correlations (R_m) between the functional connectivity density(fcd) and the estimated functional connectivity density inferred from the structural connectivity density (efcd). By using corrcoef function in matlab, the corresponding correlation coefficient p-value for each model all equal to 1, such a result indicates that the fcd and the efcd are positively correlated. In Figure 9, correlation between the modalities given by model 1-4 are strong (R_m = 0.660 +/- 0.037), whereas the latter two models are much weaker (R_m = 0.102 +/-0.046). In contradiction to the association between fcd and efcd, the direct association between fcd and the structural connectivity density (scd) are significantly poorer, as the overall correlation of the 6 models is negative and within the range of -0.180 +/- 0.037.

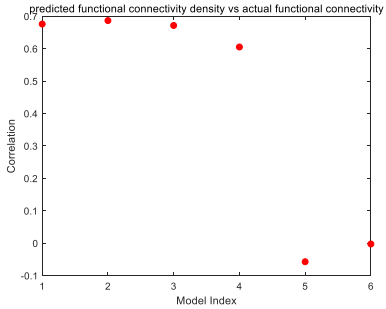

Figure 9. Plot of correlation between fcd and efcd against the model index

3.2.5 Validation of functional and structural connection relation

Figure 10 (a) shows the variation of the fitted least-squares regression coefficients(B1) for the sparse linear models of the predictor structural connection data and the response functional connection, with nonnegative regularization parameter (λ) in ascending order. An linear relation between B1 and λ was observed, with an intercept of -0.109 and gradient of 5.3226. Hence, this represents that the intrinsic coefficients of the model is -0.109 and the change in magnitude of B1 is about 5.3 times of that in λ. Such a steep change in λ and B1 slope, explains why cross-validated mean squared error(MSE) was found to be minimum at the minimum Lambda parameter (see Figure 10 b); also the observation of the dramatic increase in MSE when there is a significant increase in the order of λ in Figure 10 b.

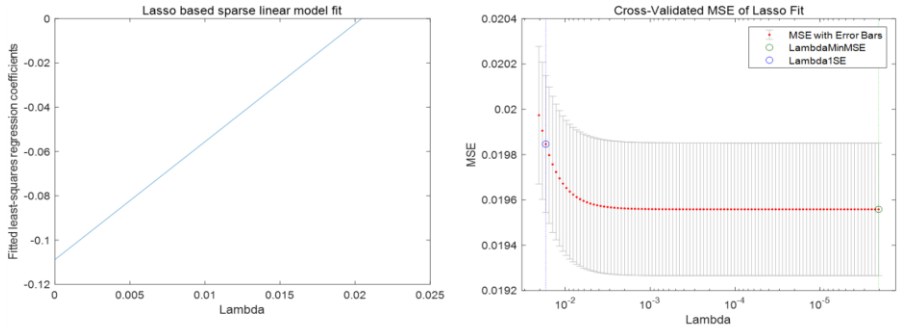

Figure 10. (a) Plot of variation of B1 obtain from Lasso based sparse linear model fit with λ. (b) Plot of variation of Cross-validated MSE of lasso fit with λ.

4. Discussion

In present study, we have developed a comprehensive analytical system to explore the properties of the graph model and investigate the relationship between the structural and the functional connectome.

The graph model's reliability was validated in terms of thresholding the FA map to observe spatial distribution variation in connectome network and quantifying the structural and the functional network's property by thresholding the graph metrics. Through the FA map thresholding, we have demonstrated that the number of remaining connectomes decreased exponentially with the applied threshold. The remaining connectomes were found to be those with higher FA intensity, and this is in agreement with Clayden's study where the highly linearised regions like white matter and the edges in the brain are more likely to remain (Clayden et al, 2011). This feature will be useful for further clinical application like studying the brain's radiation dose distribution for dw-MRI guided radiotherapy. Meanwhile, the previous observed overall trend variation of the graph metrics, implies the threshold value applied to each connectivity weight has direct impact on the network's structure. In general, the higher the threshold value applied to the connectivity weight, the graph metrics of the network structure tend to be smaller, and vice versa for the shortest path for functional connectome. This finding matches with the previous observation of spatial distribution of FA voxels above threshold value. As for the mean short path, at higher threshold value, the decreasing trend for structural connectome means the network tend to be more random and complex; whereas, the network tend to be more regular for functional connectome. A similar study done by Takagi, has same findings regards to the graph metrics variation with the applied threshold value as this study. Compared to Takagi's relevant work, the present study provides a more versatile network measurement methods, as his work only covers the measurements from the functional connectome (Takagi 2017).

The relationship between the two connectomes were probed by using the 5 basic models and the additional combined model. To explore the connectome relationship, the indirect structural connectivity was initially calculated so that it can be used for the following data fitting; Subsequently, the data fitting was performed across each edges and performed with single coefficients over all edges for each model and for each subject independently; Each type of data fitting was assessed with the AIC and BIC criteria evaluation to find the relation of the estimated model to true model, LOO_XVE and RSS evaluation was also used to evaluate the quality of points fitting simultaneously. Model 1 and model 3 were found to be the best fitting models across different edges and over all edges, in terms of AIC

and BIC. Considering their characteristics of having smallest number of parameters, we can infer that the number of parameters (k_m) occupies a very important position in minimising the relative distance between the empirical data and the predicted data and maximising the posterior probability of being true model. For RSS evaluation, the models with larger number of parameter and contain t_{ij} was found to have generally smaller RSS, for fitting across each edge. Whereas, for fitting over all edges, the models are more likely to produce smaller RSS with the probability of the corresponding terms ranked as $s_{ij} > s_{ij}^2 > t_{ij} > t_{ij}^2$. Hence, indirect structural connectome and structural connectome are more suitable to use for fitting across each edge and for fitting with single coefficients over all edge respectively, so that a higher accuracy of the fitting results will be given. Then, a novel evaluation method including the above edge-wised evaluation combined with previous subject-wised evaluation, has great potentials in applications of detecting small and early infarcts and localising stroke and intracranial haemorrhage (Srinivasan et al, 2006).

Finally, the association among the structural connection, the predicted and the empirical functional connection was found based on connectivity vertex density estimation. The strong association was only found between the fcd and the efcd produced by the models (1-4) that use either direct or indirect scd as inputs. Even though, the poor correlation results produced by models 5 and 6, are still better than that between fcd and scd. This represents that the degree of purity of scd affect the correlation level between fcd and efcd, and the overall association can be much improved by using models rather than directly using scd and fcd. Each functional connection was related to its subset of structural connections by using LASSO based sparse linear model fitting, and such model's stability was examined by cross-validation. The fitted least-squares regression coefficients (B1) and its cross-validated MSE, was demonstrated to be proportional to lambda. By varying the threshold value that simulating different brain activity level, λ, B1 and MSE can be determined according to the corresponding fit in Figure 10. The obtained B1 and MSE can be used to quantify the level of relation between the structural and functional connection. Quantifying the connection relation allows us to know the dynamic changes of activity level in brain function with the structural changes.

There are some limitations with our works. First, all the models performed poorly among the structurally unconnected regions, as the corresponding regions in structural connection matrix were not properly handled. This causes noises to our model fitting. Second, edges with negative correlations with absolute value greater than 0.1 were retained, this will result in the elevation of brain activity level (NMDA action) in those edges (Gonzales et al, 2016). Third, even the devised model has shown the best performance in terms of data fitting accuracy, representing good alignment of estimated and actual brain parcellations, its AIC and BIC are extraordinarily large which means that the estimated data are very likely to be not true. A perfect model cannot be found among the involving six models, as there is not a single model that has best value in every evaluation method.

In summarizing the discussion above, a new system performing quantification and analysis tasks of graph model's properties and relation between structural and functional connectomes has been developed. Our results support reliability and stability of the computation and evaluation functions of the system. Each function's relation to the brain structure and function, their potential clinical application and the limitations that they have also been illustrated. Models in this system do not give perfect results, and the associated noises and missing edges are not handled properly. Therefore, a further refined system is needed.

Reference

Basser, P.J., Mattiello, J., & LeBihan, D.. (1994). Estimation of the effective self-diffusion tensor from the NMR spin echo. *Journal of Magnetic Resonance Series B*, **103**(3):247-54. http://dx.doi.org/10.1006/jmrb.1994.1037

Biswal, B. , Yetkin, F. Z. , Haughton, V. M. , & Hyde, J. S. . (1995). Functional connectivity in the motor cortex of resting human brain using echo-planar mri. *Magnetic Resonance in Medicine,***34**(4): 537-541. https://doi.org/10.1002/mrm.1910340409

Bullmore, E. , & Sporns, O. . (2009). Complex brain networks: graph theoretical analysis of structural and functional systems. *Nature Reviews Neuroscience,* **10**(3): 186-198. https://doi.org/10.1038/nrn2575

Chen, X. & Wang Y.J. Predicting resting-state functional connectivity with efficient structural connectivity. *IEEE/CAA Journal of Automatica Sinica*, 5(6): 1079-1088.
https://doi.org/10.1109/JAS.2017.7510880

Clayden, J.D.. (2013). Imaging connectivity: mri and the structural networks of the brain. *Functional Neurology,* **28**(3), 197. https://doi.org/10.11138/FNeur/2013.28.3.197

Contreras, J. A. , Joaquín Goñi, Risacher, S. L. , Sporns, O. , & Saykin, A. J. . (2015). The structural and functional connectome and prediction of risk for cognitive impairment in older adults. *Current Behavioral Neuroscience Reports,* **2**(4): 234-245.
https://dx.doi.org/10.1007%2Fs40473-015-0056-z.

Deco, G. , Ponce-Alvarez, A. , Mantini, D. , Romani, G. L. , Hagmann, P. , & Corbetta, M. . (2013). Resting-state functional connectivity emerges from structurally and dynamically shaped slow linear fluctuations. *Journal of Neuroscience,***33**(27), 11239-11252.
https://doi.org/10.1523/JNEUROSCI.1091-13.2013

Deligianni, F., Centeno, M. , Carmichael, D. W. , & Clayden, J. D. . (2014). Relating resting-state fmri and eeg whole-brain connectomes across frequency bands. *Frontiers in Neuroscience,* **8**(258). https://dx.doi.org/10.3389%2Ffnins.2014.00258

Deligianni F., Varoquaux G., Thirion B., Sharp D.J., Ledig C., Leech R. & Rueckert D. (2013). A framework for inter-subject prediction of functional connectivity from structural networks.
IEEE Transactions on Medical Imaging, **32**(12):2200–2214.
https://doi.org/10.1109/TMI.2013.2276916

Watts, D. J. , & Strogatz, S. H. . (1998). Collective dynamics of 'small-world' networks. *Nature.* **393**: 440–442. https://doi.org/10.1038/30918

Fabozzi, F. J. , Focardi, S. M. , Rachev, S. T. , & Arshanapalli, B. G. . (2014). Appendix E: Model Selection Criterion: AIC and BIC. The Basics of Financial Econometrics: Tools, Concepts, and Asset Management Applications. John Wiley & Sons, Inc.
https://onlinelibrary.wiley.com/doi/pdf/10.1002/9781118856406.app5

Fagiolo, G. (2007). Clustering in complex directed networks. *Physical Review. E.* **76**, 026107. https://doi.org/10.1103/PhysRevE.76.026107

Fjell, A. M. , Sneve, M. H. , Håkon Grydeland, Storsve, A. B. , Amlien, I. K. , & Yendiki, A. , et al. (2017). Relationship between structural and functional connectivity change across the adult lifespan: a longitudinal investigation. *Human Brain Mapping,***38**(1): 561.
https://dx.doi.org/10.1002%2Fhbm.23403

Honey, C. J. , Sporns, O. , Cammoun, L. , Gigandet, X. , Thiran, J. P. , & Meuli, R. , et al. (2009). Predicting human resting-state functional connectivity from structural connectivity. *PROCEEDINGS OF THE NATIONAL ACADEMY OF SCIENCES OF THE UNITED STATES OF AMERICA,* **106**(6), 2035-2040. https://dx.doi.org/10.1073%2Fpnas.0811168106

J.D. Clayden, S. Muñoz Maniega, A.J. Storkey, M.D. King, M.E. Bastin & C.A. Clark (2011). TractoR: Magnetic resonance imaging and tractography with R. *Journal of Statistical Software* **44**(8):1–18.

Latora, V. , & Marchiori, M. . (2001). Efficient behavior of small-world networks. *Physical Review Letters,* **87**(19), 198701. https://doi.org/10.1103/PhysRevLett.87.198701

Nicole R. Gonzales & James C. Grotta(2016). 55 - Pharmacologic Modification of Acute Cerebral Ischemia, *Stroke (Sixth Edition)*, Elsevier: 916-936.e5, https://doi.org/10.1016/B978-0-323-29544-4.00055-4.

Rubinov M. & Sporns O. (2010). Complex network measures of brain connectivity: Uses and interpretations. *NeuroImage* **52**:1059–1069. https://doi.org/10.1016/j.neuroimage.2009.10.003

Schäfer J. & Strimmer K. (2005). A shrinkage approach to large-scale covariance matrix estimation and implications for functional genomics. *Statistical Applications in Genetics and Molecular Biology* **4**(1):32. https://doi.org/10.2202/1544-6115.1175

Shi, Y. , & Toga, A. W. . (2017). Connectome imaging for mapping human brain pathways. *Molecular Psychiatry*. **22**, 1230–1240. https://doi.org/10.1038/mp.2017.92

Sinke, M. R. T. , Otte, W. M. , Christiaens, D. , Schmitt, O. , & Dijkhuizen, R. M. . (2018). Diffusion mri-based cortical connectome reconstruction: dependency on tractography procedures and neuroanatomical characteristics. *Brain Structure and Function,* **223**(5), 2269-2285. https://dx.doi.org/10.1007%2Fs00429-018-1628-y

Srinivasan A, Goyal M, Al azri F et-al. State-of-the-art imaging of acute stroke. Radiographics. 2006;26 Suppl 1 : S75-95. doi:10.1148/rg.26si065501

Takagi K. (2017). A distribution model of functional connectome based on criticality and energy constraints. *PloS one*, *12*(5), e0177446. doi:10.1371/journal.pone.0177446

Woolrich, M. W., Ripley, B. D., Brady, M., & Smith, S. M. (2001). Temporal Autocorrelation in Univariate Linear Modeling of FMRI Data. NeuroImage, **14**(6), 1370–1386. http://doi.org/10.1006/nimg.2001.0931